ADVANCED MATERIALS

www.advmat.de

Mixed Valence Perovskite $Cs_2Au_2I_6$: A Potential Material for Thin-Film Pb-Free Photovoltaic Cells with Ultrahigh Efficiency

Lamjed Debbichi, Songju Lee, Hyunyoung Cho, Andrew M. Rappe, Ki-Ha Hong, Min Seok Jang, and Hyungjun Kim**

New light is shed on the previously known perovskite material, $Cs_2Au_2I_6$, as a potential active material for high-efficiency thin-film Pb-free photovoltaic cells. First-principles calculations demonstrate that $Cs_2Au_2I_6$ has an optimal band gap that is close to the Shockley–Queisser value. The band gap size is governed by intermediate band formation. Charge disproportionation on Au makes $Cs_2Au_2I_6$ a double-perovskite material, although it is stoichiometrically a single perovskite. In contrast to most previously discussed double perovskites, $Cs_2Au_2I_6$ has a direct-band-gap feature, and optical simulation predicts that a very thin layer of active material is sufficient to achieve a high photoconversion efficiency using a polycrystalline film layer. The already confirmed synthesizability of this material, coupled with the state-of-the-art multiscale simulations connecting from the material to the device, strongly suggests that $Cs_2Au_2I_6$ will serve as the active material in highly efficient, nontoxic, and thin-film perovskite solar cells in the very near future.

In the last few years, a highly intensive search has been conducted for novel materials that can serve as a platform for optoelectronic devices with higher efficiency that are environmentally friendly. In particular, the search for sources of clean energy has stimulated researches on materials and architectures for next-generation solar cells. Due to their outstanding photophysical and electronic transport properties,[1–3] hybrid and inorganic lead halide perovskites have emerged as a promising new class of base materials for optoelectronics applications. The progress in the performance of hybrid perovskite solar cells has been rapid, with recent reports of certified photoconversion efficiency (PCE) over 20%.[4] It is further noted that their theoretical maximum is greater than 30%, which is even higher than the theoretical maximum efficiency of silicon (27%),[5] suggesting more room for efficiency enhancement. Despite their superior properties as photovoltaic (PV) materials, organic–inorganic hybrid lead halide perovskites suffer from two major concerns: stability and toxicity issues. This stimulates many researchers to find a new material that is purely inorganic (for enhanced stability) and free of toxic lead.

Recently, trivalent metal cations such as Bi and Sb attract much attention as potential candidates for nontoxic metal cations, and there have been several successful syntheses of trivalent metal based perovskites such as $MA_3Bi_2I_9$,[6] $Cs_3Bi_2I_9$,[7] and $Cs_3Sb_2I_9$ (where MA = CH_3NH_3).[8] Although they show better stability than $MAPbI_3$, the $A_3^IM_2^{III}X_9$ type perovskites show wide band gaps of >1.9 eV, originating from their reduced structural dimensionality,[9] which significantly degrades the photovoltaic efficiency. In order to retain the 3D corner sharing octahedron structure of the cubic perovskites, which is deemed to be essential for the optimal band gap and isotropic carrier transport characteristics, double-perovskite-type lattice structures like $A^I_2M^IM^{III}X_6$ (where M^{III} is usually Bi^{III} or In^{III}) have recently been explored by several groups by means of simulations and experiments.[10–16] In their seminal work, Volonakis et al. suggested several double perovskites using a computational materials screening technique, and succeeded to synthesize $Cs_2BiAgCl_6$.[16] However, the BiAg-based double perovskites have wide indirect band gaps due to angular momentum mismatch of frontier orbitals,[17] resulting in unsatisfactory photovoltaic performance. Zhao et al. also suggested that new double perovskite materials $Cs_2In^ISb^{III}Cl_6$ and $Cs_2In^IBi^{III}Cl_6$ would have a proper band gap size and a direct band gap, based on their computational

Dr. L. Debbichi, Prof. H. Kim
Graduate School of EEWS
Korea Advanced Institute of Science and Technology (KAIST)
291 Daehak-Ro, Yuseong-Gu, Daejeon 34141, Korea
E-mail: linus16@kaist.ac.kr

S. Lee, H. Cho, Prof. M. S. Jang
School of Electrical Engineering
Korea Advanced Institute of Science and Technology (KAIST)
291 Daehak-Ro, Yuseong-Gu, Daejeon 34141, Korea
E-mail: jang.minseok@kaist.ac.kr

Prof. A. M. Rappe
Department of Chemistry
University of Pennsylvania
Philadelphia, PA 19104-6323, USA

Prof. K.-H. Hong
Department of Materials Science and Engineering
Hanbat National University
125 Dongseo-Daero, Yuseong-Gu, Daejeon 34158, Korea

Prof. H. Kim
Department of Chemistry
Korea Advanced Institute of Science and Technology (KAIST)
291 Daehak-Ro, Yuseong-Gu, Daejeon 34141, Korea

The ORCID identification number(s) for the author(s) of this article can be found under https://doi.org/10.1002/adma.201707001.

DOI: 10.1002/adma.201707001

materials screening.[18] However, it should be noted that In^{I}-based double perovskites are known to be susceptible to oxidation into In^{III}-based compounds, degrading their chemical stability.[13] Thus, there still exists a strong demand for finding materials with a proper band gap (<1.5 eV), direct band gap feature, and substantial thermodynamic stability.

Here, we analyze the previously discovered perovskite material, $Cs_2Au_2X_6$ (X = Cl, Br, I), which is free of organic molecules and lead and investigate its suitability for application in thin-film photovoltaic and related optoelectronic devices. The structure of this material has been known for more than two decades.[19,20] Using first-principles density functional theory (DFT) calculations, we demonstrate that the Au atoms have mixed valency of +1 and +3, in agreement with previous reports.[21] This disproportionation allows this ternary compound to inherit the merits of the previously suggested double perovskite materials based on quaternary elements, such as an optimal band gap size. Using optical simulations, we assess the suitability of this material as an absorbing layer for solar cells, predicting a PCE higher than organic–inorganic hybrid lead halide perovskites at the device level.

Figure 1a shows the structure of the $Cs_2Au_2X_6$ (X = Cl, Br, I) perovskite family. At room temperature, $Cs_2Au_2X_6$ crystallizes in a distorted tetragonal mixed-valence perovskite structure with space group I4/mmm,[22] and the Au cations undergo charge disproportionation,[21] with Au^{I} and Au^{III} oxidation states in a rocksalt ordering. The associated differences in coordination of gold atoms due to octahedral cage breathing suggest a formal valence assignment AuX_2 and AuX_4 alternating through the crystal. Of course, both Au^{I} and Au^{III} are surrounded by six halogen atoms, retaining a 3D distorted corner-shared octahedral network (Figure 1b). Furthermore, it is worth noting that high hydrostatic pressure leads the $Cs_2Au_2X_6$ structure to undergo a structural transition that is accompanied by a semiconductor-to-metal transition. Pressure symmetrizes the Au^{I} and Au^{III} sites, yielding a single-valence state of Au^{II}.[23,24]

In Figure 1c, we show the calculated electronic band structure of $Cs_2Au_2I_6$ using two different choices of DFT methods of PBE and HSE, yielding a direct band gap near the N point of the Brillouin zone (Figure 1d). As is widely known, the GGA-PBE band gap (0.79 eV) is likely an underestimate, while the computationally more expensive screened hybrid functional HSE yields a band gap of 1.21 eV that is considered more reliable and is also comparable to the experimental optical gap of 1.31 eV.[21] However, there are no significant differences between the PBE and HSE results in terms of band dispersion, allowing the usual scissoring approach to correct the PBE band structure.

An interesting feature of the band structure is the formation of an isolated intermediate band (IB) between the valence band (VB) and conduction band (CB). Such a unique electronic structure has often been reported in double perovskites due to the trivalent B-site metals,[25–27] and it has been exploited to obtain reduced band gaps in the range of 1.1–1.4 eV for high-performance solar cells. Similar to these double perovskites, the IB of $Cs_2Au_2I_6$ is also from the trivalent cations—an antibonding hybridization of Au^{III} d_{x2-y2} orbital and I p orbital (Figure S1, Supporting Information).[28] This leads to an optimal size of direct band gap, implying that $Cs_2Au_2I_6$ could have optimal material properties as an active layer in thin film solar cells.

Beyond analysis of electronic band structure and band gap size, we adopted a multiscale simulation strategy to evaluate the photophysical properties of $Cs_2Au_2I_6$. From first-principles simulations, we first calculated the frequency-dependent complex dielectric function in **Figure 2**, which was then transferred to larger-scale electromagnetic wave simulations and various optical analyses. The detailed computational procedure is fully described in the Experimental Section, which is designed for an efficient and accurate calculation of the dielectric functions from the first-principles calculations.

Following the shape of the IB (Figure S2, Supporting Information), the optical properties are found to be highly anisotropic with respect to the relative orientation of the optical polarization of light (E) and the crystal lattice, with maximum response when the electric field is perpendicular to the c-axis. For $E \perp c$, the calculated ε'' shows two principal peaks at 1.49 and 1.83 eV, which are well aligned with the solar spectrum, whereas for $E \,//\, c$, the optical response is relatively weak. These

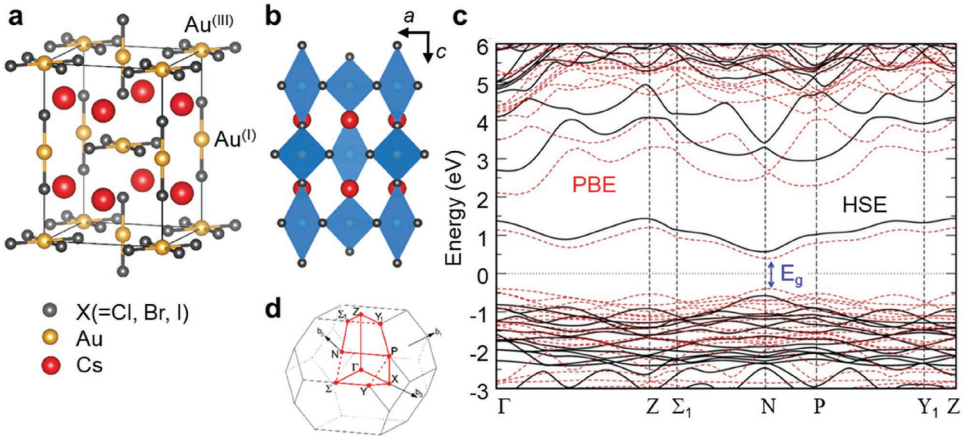

Figure 1. Crystal structure of the mixed-valence perovskite $Cs_2Au_2X_6$ (X = Cl, Br, I): a) square planar AuX_4 and linear chain AuX_2 complexes are formed due to the mixed valency of $Au^{(III)}$ and $Au^{(I)}$, which b) leads to the alternating elongated and compressed AuX_6 octahedra. The Cs, Au, and X atoms are shown with red, gold, and gray spheres, respectively. c) DFT-calculated electronic band structure using the PBE-GGA functional (red) and the HSE hybrid functional (black), where d) the corresponding first Brillouin zone is shown with the selected high-symmetry k-points labeled.

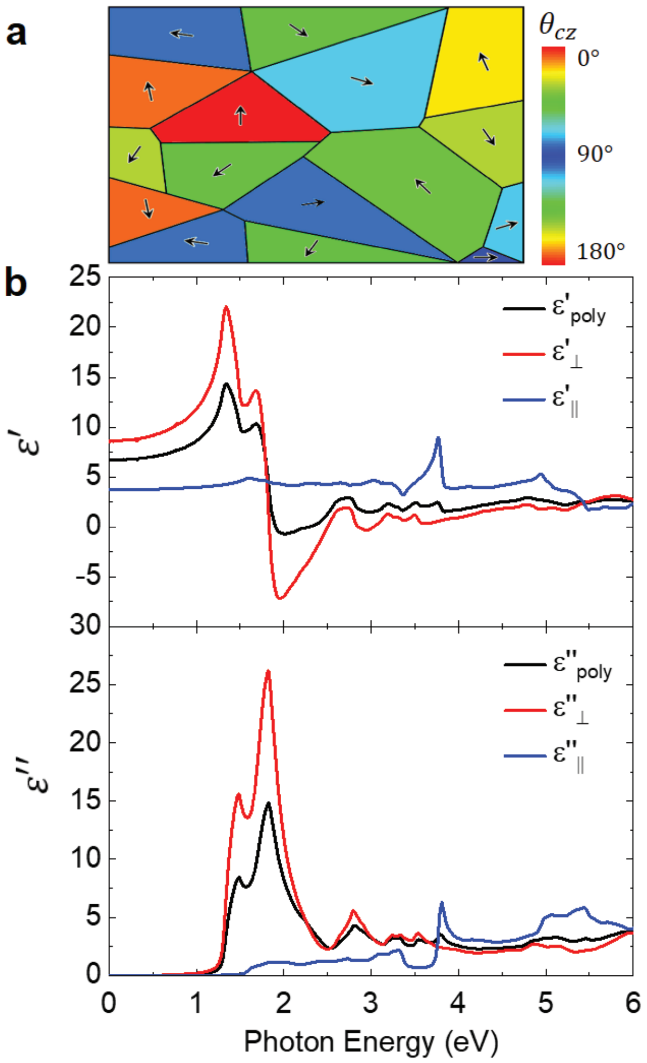

Figure 2. a) Schematic of polycrystal $Cs_2Au_2I_6$ composed of fine grains of random crystal orientations. The crystal orientation of each grain is specified by θ_{cz}, the polar angle between the vertical axis and the optical axis. b) Real (ε') and imaginary (ε'') part of electric permittivity of single-crystalline (red curve for $E \perp c$ and blue curve for E // c) and polycrystalline (black curve) $Cs_2Au_2I_6$ as functions of photon energy.

results are in good agreement with the experimental optical reflectivity measurements[21] at room temperature. It is further noted that the low-energy absorptions below ≈3 eV are attributed to the intermolecular 5d–5d transitions between the Au^+ and Au^{3+} ions involving the IB, while the high-energy absorptions are associated with the intramolecular 5d-6s transitions of AuI_4^- and AuI_2^- molecules, respectively.[29]

Strong optical anisotropy implies that the photoabsorption can be maximized by aligning the crystal orientation to the light incidence direction. We note that the single-crystal synthesis of $Cs_2Au_2I_6$ has already been demonstrated experimentally using a self-flux method, albeit the crystalline quality could perhaps be further improved.[30] Conveniently, the single-crystal $Cs_2Au_2I_6$ is found to grow such that its optical axis is perpendicular to the substrate plane, and therefore should naturally exhibit maximum photoabsorption for normally incident light.

In addition to the optical properties of single-crystal $Cs_2Au_2I_6$, we also evaluate the dielectric functions of polycrystalline $Cs_2Au_2I_6$ composed of fine grains with random crystal orientations as illustrated in Figure 2a. Unlike single-crystal $Cs_2Au_2I_6$ which exhibits a large anisotropy, the polycrystalline $Cs_2Au_2I_6$ can be described as a homogeneous medium having an isotropic dielectric function ε_{poly} by using the effective medium theory[31]

$$\frac{\varepsilon_x-\varepsilon_{poly}}{\varepsilon_x+2\varepsilon_{poly}}+\frac{\varepsilon_y-\varepsilon_{poly}}{\varepsilon_y+2\varepsilon_{poly}}+\frac{\varepsilon_z-\varepsilon_{poly}}{\varepsilon_z+2\varepsilon_{poly}}=0 \quad (1)$$

Because $Cs_2Au_2I_6$ is uniaxial material, namely, $\varepsilon_x = \varepsilon_y = \varepsilon_\perp$ and $\varepsilon_z = \varepsilon_\parallel$, this formula reduces to $\varepsilon_{poly}=\frac{1}{4}\left[\varepsilon_\perp+\sqrt{\varepsilon_\perp^2+8\varepsilon_\perp\varepsilon_\parallel}\right]$ and the resulting ε_{poly} is shown in Figure 2b. As expected, the polycrystalline $Cs_2Au_2I_6$ has moderate refractive indices, frequency-dependent permittivity between $\varepsilon_\perp$ and $\varepsilon_\parallel$, and light absorption across the entire solar spectrum.

In order to assess $Cs_2Au_2I_6$ as a potential photovoltaic material, we quantitatively compare it with a lead halide perovskite, $MAPbI_3$,[32] presently the most studied perovskite material for solar cell applications. **Figure 3** compares the solar irradiance spectrum of Air Mass 1.5 Global (AM1.5G) and the absorption coefficients (α) of single-crystal and polycrystalline $Cs_2Au_2I_6$ and $MAPbI_3$. Here, for the single-crystal $Cs_2Au_2I_6$, the wavevector of light is assumed to be along the crystal c-axis (i.e., $E \perp c$). Due to the lower band gap of 1.31 eV, both single-crystal and polycrystalline $Cs_2Au_2I_6$ exhibit absorption spectra better matched to the solar irradiance spectrum than $MAPbI_3$, whose band gap is 1.55 eV.

We calculate the short-circuit current densities (J_{sc}) of the single and polycrystalline $Cs_2Au_2I_6$ and $MAPbI_3$ assuming single-path absorption and unity internal quantum efficiency

$$J_{sc}=e\int_{\lambda_{min}}^{\lambda_g}\frac{\mathrm{AM1.5G}(\lambda)\times(1-\exp(-\alpha d))}{hc/\lambda}\mathrm{d}\lambda \quad (2)$$

where e is the elementary charge, d is the propagation distance that can be interpreted as the thickness of the material. The numerical integrations were performed in the range from

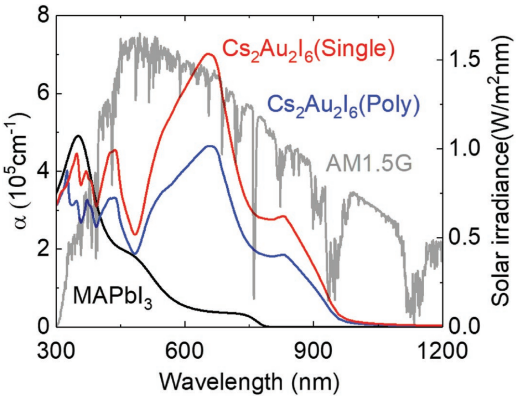

Figure 3. Solar irradiance spectrum (gray) and absorption coefficient of single (red) and poly (blue) crystal $Cs_2Au_2I_6$ and $MAPbI_3$ (black) versus wavelength of light.

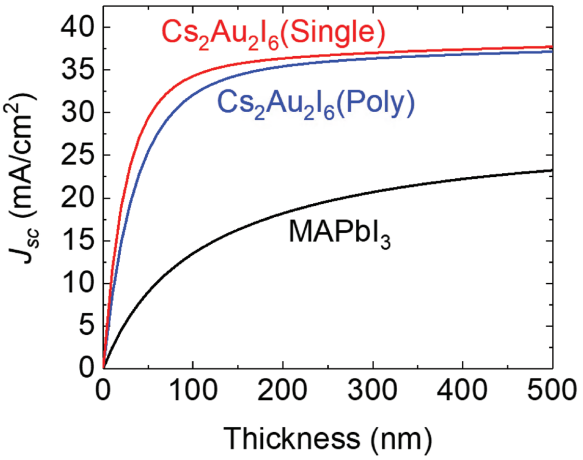

Figure 4. Dependence of the short-circuit current density of single (red) and poly (blue) crystal $Cs_2Au_2I_6$ and $MAPbI_3$ (black) on the thickness of the material, assuming single-path absorption.

λ_{min} = 280 nm to the band gap wavelength λ_g. **Figure 4** plots how J_{sc} of each material depends on thickness. The efficient absorption of $Cs_2Au_2I_6$ allows for a high level of J_{sc} in just a few tens of nm thickness. For instance, at the path length of 50 nm, the J_{sc} of single and polycrystalline $Cs_2Au_2I_6$ are 29.4 and 25.5 mA cm^{-2}, respectively, which are 2.5 times higher than that of $MAPbI_3$ (≈8.98 mA cm^{-2}). Even in large thickness limit, $Cs_2Au_2I_6$ has 1.5 times higher saturation current density (≈39.4 mA cm^{-2}) compared to $MAPbI_3$ (≈26.6 mA cm^{-2}).

Next, we examine whether the excellent photophysical material properties of $Cs_2Au_2I_6$ can be retained at the actual solar cell device level. We thus modeled a realistic full solar cell device structure incorporating electrodes and charge transfer layers by using full-wave electromagnetic simulations based on the finite element methods (FEM). For fair comparison, we adopt a widely used device structure of lead halide perovskite solar cell, consisting of glass/ITO(150 nm)/TiO_2(40 nm)/active layer(350 nm)/spiro-OMeTAD(200 nm)/Au[33] as illustrated in **Figure 5**a, where the active layer part is single or polycrystal $Cs_2Au_2I_6$, or $MAPbI_3$. The optical properties of ITO, TiO_2, and spiro-OMeTAD are adopted from Holman et al.,[34] Kim,[35] and Loper et al.,[36] respectively. Figure 5b illustrates the absorption in the active layer for different perovskite materials under normal incidence of light. Above its band gap (λ < 800 nm), $MAPbI_3$ exhibits slightly better absorption efficiency because its refractive index is better matched to the nearby carrier transfer and transparent electrode materials which results in a lower reflection loss. Especially at around 500 nm, $Cs_2Au_2I_6$ possesses an absorption dip that originates from the reflection loss. However, $MAPbI_3$ becomes inactive below its band gap (λ > 800 nm) whereas $Cs_2Au_2I_6$ materials still show strong absorption up until their band gap (λ < 946 nm) and thus have higher overall absorption. Between single and polycrystalline $Cs_2Au_2I_6$, unexpectedly, the polycrystal shows better optical absorption performance even with lower absorption coefficient (α). This is because the higher refractive index of the single-crystal $Cs_2Au_2I_6$ creates large index contrast to the neighboring layers which induces higher reflection loss, whereas the moderate index of polycrystal $Cs_2Au_2I_6$ suppresses reflection and allows for more light enter into the device. For this device structure, the estimated J_{sc} are 25.4, 29.5, and 22.6 mA cm^{-2} for single and polycrystal $Cs_2Au_2I_6$ and $MAPbI_3$ active layers, respectively. It is further noted that the polycrystalline $Cs_2Au_2I_6$ is better than the single crystal not only in optical performance but also in electrical performance. The charge carriers of the single-crystal $Cs_2Au_2I_6$ have large effective mass and therefore short diffusion length along the out-of-plane direction. Consequently, extraction of photogenerated carriers could be inefficient. In polycrystalline $Cs_2Au_2I_6$, in contrast, the grains are randomly oriented and so there should always exist paths for the fast diffusion of carriers. Therefore, we claim that polycrystalline $Cs_2Au_2I_6$ is better suited for photovoltaic applications. Conservatively estimating the open-circuit voltage (V_{oc}) of the solar cell to be 0.4 V smaller than the band gap of the active material[37] and the fill factor of 0.8,[38] polycrystalline $Cs_2Au_2I_6$ based devices could show photoconversion efficiency as high as 21.5%, which is comparable with the current state-of-the-art lead halide perovskite solar cell, and the efficiency could go even higher with optimized photonic design.

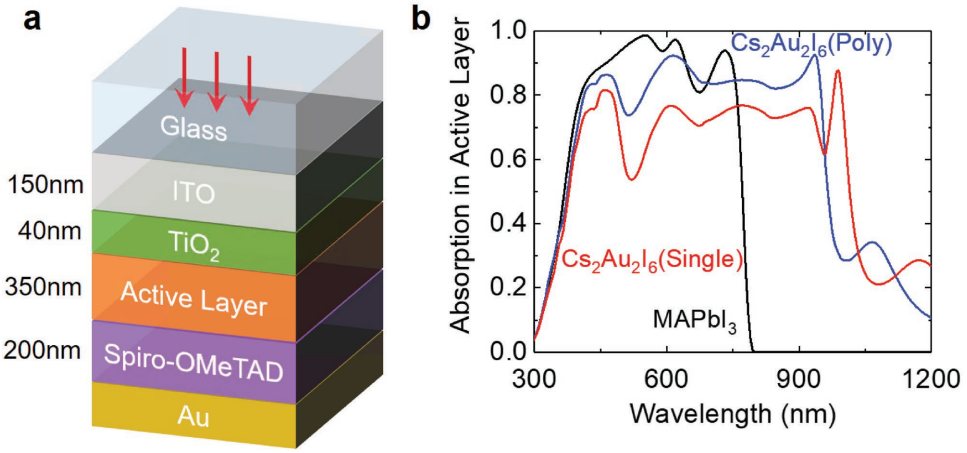

Figure 5. a) Schematic of full solar cell device structure (glass/ITO(150 nm)/TiO_2(40 nm)/active layer(350 nm)/spiro-OMeTAD(200 nm)/Au). b) Absorption in the active layer of the full devices based on single (red) and polycrystal (blue) $Cs_2Au_2I_6$ are indicated, as well as $MAPbI_3$ (black).

More interestingly, $Cs_2Au_2I_6$-based photovoltaic devices can retain their superior performance even at a 50 nm active layer thickness. For the device structure of glass/ITO(150 nm)/TiO_2(40 nm)/active layer(50 nm)/spiro-OMeTAD(70 nm)/Au, the estimated J_{sc} and the photoconversion efficiency of the $Cs_2Au_2I_6$-based device are still as high as 25.0 mA cm^{-2} and 18.2%, whereas the estimated efficiency of $MAPbI_3$-based device drops significantly to 8.7% as shown in Figure S3 (Supporting Information).

In summary, we investigate the already known perovskite material $Cs_2Au_2I_6$ for application in nontoxic thin-film solar cells. Due to the mixed-valence Au atoms on the B-site, this material resembles the double-perovskite materials in terms of electronic structure, resulting in a proper band gap size of 1.31 eV, which is close the ideal band gap for photovoltaic materials governed by the Shockley–Queisser theory. Unlike most previously discussed Pb-free perovskite solar cell materials, $Cs_2Au_2I_6$ has a direct band gap feature, enabling the use of this material even as an ≈50 nm thin film, preserving the high optical absorption. Our further in-depth optical simulation confirms that the ideal materials properties can be achieved for polycrystalline $Cs_2Au_2I_6$, which can be successfully transferred into the device level, where 30 mA cm^{-2} of short-circuit current and over 20% photoconversion efficiency are predicted. As this material has already been synthesized even in the single-crystalline quality, we anticipate that this study will immediately stimulate experimentalists to produce and test thin-film photovoltaic cells based on $Cs_2Au_2I_6$.

Computational Methods

DFT Calculations: All calculations are performed using the Vienna ab initio Simulation Package (VASP)[39] with the projected augmented wave (PAW) potentials.[40] The Perdew, Burke, and Ernzerhof (PBE)[41] exchange-correlation functional was employed to perform full structural optimization. The kinetic energy cutoff for the plane wave basis set was chosen to be 700 eV with a Γ-centered k-point mesh of $14 \times 14 \times 10$ used to optimize crystal structure with PBE. All structures are fully relaxed until the total energies are converged up to 10^{-5} eV and the Hellmann–Feynman forces are less than 0.001 eV $Å^{-1}$. PBE optimized cell parameters and structural information (e.g., Au–I distances) are listed in Table S1 (Supporting Information), which agree well with the experimental values.

Due to the well-known difficulties of standard DFT in predicting the band gaps of semiconductors, the hybrid density functional method based on the Heyd–Scuseria–Ernzerhof (HSE) scheme[42,43] was also used to calculate the electronic structure using the PBE optimized structures. For the HSE calculations, reduced $8 \times 8 \times 6$ k-point mesh was employed due to the larger computational cost than PBE calculations.

The optical properties were calculated using the random phase approximation implemented in VASP.[44]

To calculate the frequency-dependent dielectric functions in an effective and reliable manner, the computational procedure is outlines as follows:

(1) Calculate the imaginary dielectric function, ε'' from the PBE electronic ground state with extensive sampling of reciprocal space using $18 \times 18 \times 12$ mesh.
(2) Shift the ε'' by the difference of PBE band gap and the experimentally measured band gap (i.e., 0.52 eV) in order to resolve the well-known band gap underestimation problem of PBE.
(3) Calculate the real dielectric function ε' by numerically solving the Kramers–Kronig transformation.

The shifting operation of the ε'' is equivalent to the usual scissoring approach of the conduction bands. In order to demonstrate the robustness of this conclusion, another set of simulations were also performed using the ε'' shifted by 0.42 eV (reproducing the HSE band gap instead of experimental gap) in Figures S4 and S5 (Supporting Information), showing almost no difference from Figures 2–4.

Supporting Information

Supporting Information is available from the Wiley Online Library or from the author.

Acknowledgements

L.D. and S.L. contributed equally to this work. This work was supported by the Creative Materials Discovery Program (Grant Nos. 2017M3D1A1039378 and 2016M3D1A1900038), and also by the Global Frontier R&D Program (2013M3A6B1078884) through the National Research Foundation of Korea (NRF) funded by the Ministry of Science and ICT. A.M.R. acknowledges support from the National Science Foundation, under Grant No. DMR-1719353.

Conflict of Interest

The authors declare no conflict of interest.

Keywords

first-principles calculations, lead-free perovskite solar cells, mixed valency, multiscale simulations, thin film solar cells

Received: November 30, 2017
Revised: December 19, 2017
Published online: February 6, 2018

[1] G. C. Xing, N. Mathews, S. Y. Sun, S. S. Lim, Y. M. Lam, M. Gratzel, S. Mhaisalkar, T. C. Sum, *Science* **2013**, *342*, 344.
[2] S. D. Stranks, G. E. Eperon, G. Grancini, C. Menelaou, M. J. P. Alcocer, T. Leijtens, L. M. Herz, A. Petrozza, H. J. Snaith, *Science* **2013**, *342*, 341.
[3] G. E. Eperon, T. Leijtens, K. A. Bush, R. Prasanna, T. Green, J. T. W. Wang, D. P. McMeekin, G. Volonakis, R. L. Milot, R. May, A. Palmstrom, D. J. Slotcavage, R. A. Belisle, J. B. Patel, E. S. Parrott, R. J. Sutton, W. Ma, F. Moghadam, B. Conings, A. Babayigit, H. G. Boyen, S. Bent, F. Giustino, L. M. Herz, M. B. Johnston, M. D. McGehee, H. J. Snaith, *Science* **2016**, *354*, 861.
[4] W. S. Yang, J. H. Noh, N. J. Jeon, Y. C. Kim, S. Ryu, J. Seo, S. I. Seok, *Science* **2015**, *348*, 1234.
[5] T. A. Berhe, W. N. Su, C. H. Chen, C. J. Pan, J. H. Cheng, H. M. Chen, M. C. Tsai, L. Y. Chen, A. A. Dubale, B. J. Hwang, *Energy Environ. Sci.* **2016**, *9*, 323.
[6] M. Q. Lyu, J. H. Yun, M. L. Cai, Y. L. Jiao, P. V. Bernhardt, M. Zhang, Q. Wang, A. J. Du, H. X. Wang, G. Liu, L. Z. Wang, *Nano Res.* **2016**, *9*, 692.
[7] B. W. Park, B. Philippe, X. L. Zhang, H. Rensmo, G. Boschloo, E. M. J. Johansson, *Adv. Mater.* **2015**, *27*, 6806.
[8] B. Saparov, F. Hong, J. P. Sun, H. S. Duan, W. W. Meng, S. Cameron, I. G. Hill, Y. F. Yan, D. B. Mitzi, *Chem. Mater.* **2015**, *27*, 5622.

[9] K. H. Hong, J. Kim, L. Debbichi, H. Kim, S. H. Im, *J. Phys. Chem. C* **2017**, *121*, 969.
[10] A. H. Slavney, T. Hu, A. M. Lindenberg, H. I. Karunadasa, *J. Am. Chem. Soc.* **2016**, *138*, 2138.
[11] E. T. McClure, M. R. Ball, W. Windl, P. M. Woodward, *Chem. Mater.* **2016**, *28*, 1348.
[12] K. Z. Du, W. W. Meng, X. M. Wang, Y. F. Yan, D. B. Mitzi, *Angew. Chem., Int. Ed.* **2017**, *56*, 8158.
[13] Z. W. Xiao, K. Z. Du, W. W. Meng, J. B. Wang, D. B. Mitzi, Y. F. Yan, *J. Am. Chem. Soc.* **2017**, *139*, 6054.
[14] F. X. Wei, Z. Y. Deng, S. J. Sun, F. H. Zhang, D. M. Evans, G. Kieslich, S. Tominaka, M. A. Carpenter, J. Zhang, P. D. Bristowe, A. K. Cheetham, *Chem. Mater.* **2017**, *29*, 1089.
[15] M. R. Filip, S. Hillman, A. A. Haghighirad, H. J. Snaith, F. Giustino, *J. Phys. Chem. Lett.* **2016**, *7*, 2579.
[16] G. Volonakis, M. R. Filip, A. A. Haghighirad, N. Sakai, B. Wenger, H. J. Snaith, F. Giustino, *J. Phys. Chem. Lett.* **2016**, *7*, 1254.
[17] C. N. Savory, A. Walsh, D. O. Scanlon, *ACS Energy Lett.* **2016**, *1*, 949.
[18] X. G. Zhao, J. H. Yang, Y. H. Fu, D. W. Yang, Q. L. Xu, L. P. Yu, S. H. Wei, L. J. Zhang, *J. Am. Chem. Soc.* **2017**, *139*, 2630.
[19] N. Kojima, M. Hasegawa, H. Kitagawa, T. Kikegawa, O. Shimomura, *J. Am. Chem. Soc.* **1994**, *116*, 11368.
[20] N. Matsushita, H. Kitagawa, N. Kojima, *Acta Crystallogr., C* **1997**, *53*, 663.
[21] X. J. Liu, K. Matsuda, Y. Moritomo, A. Nakamura, N. Kojima, *Phys. Rev. B* **1999**, *59*, 7925.
[22] W. Denner, H. Schulz, H. Damour, *Acta Crystallogr., A* **1979**, *35*, 360.
[23] B. Winkler, C. J. Pickard, M. D. Segall, V. Milman, *Phys. Rev. B* **2001**, *63*, 214103.
[24] M. Trigo, J. Chen, M. P. Jiang, W. L. Mao, S. C. Riggs, M. C. Shapiro, I. R. Fisher, D. A. Reis, *Phys. Rev. B* **2012**, *85*, 081102(R).
[25] X.-G. Zhao, D. Yang, Y. Sun, T. Li, L. Zhang, L. Yu, A. Zunger, *J. Am. Chem. Soc.* **2017**, *139*, 6718.
[26] J. Xu, J.-B. Liu, B.-X. Liu, B. Huang, *J. Phys. Chem. Lett.* **2017**, *8*, 4391.
[27] L. Jiang, I. Grinberg, F. Wang, S. M. Young, P. K. Davies, A. M. Rappe, *Phys. Rev. B* **2014**, *90*, 075153.
[28] A. V. Ushakov, S. V. Streltsov, D. I. Khomskii, *J. Phys.: Condens. Matter* **2011**, *23*, 445601.
[29] N. Kojima, H. Kitagawa, *J. Chem. Soc., Dalton Trans.* **1994**, 327.
[30] S. C. Riggs, M. C. Shapiro, F. Corredor, T. H. Geballe, I. R. Fisher, G. T. McCandless, J. Y. Chan, *J. Cryst. Growth* **2012**, *355*, 13.
[31] G. W. Milton, *The Theory of Composites*, Cambridge University Press, Cambridge, UK **2002**.
[32] P. Loper, M. Stuckelberger, B. Niesen, J. Werner, M. Filipic, S. J. Moon, J. H. Yum, M. Topic, S. De Wolf, C. Ballif, *J. Phys. Chem. Lett.* **2015**, *6*, 66.
[33] N. E. Gorji, H. Sohrabpoor, *Mater. Lett.* **2016**, *177*, 143.
[34] Z. C. Holman, M. Filipic, A. Descoeudres, S. De Wolf, F. Smole, M. Topic, C. Ballif, *J. Appl. Phys.* **2013**, *113*, 013107.
[35] S. Y. Kim, *Appl. Opt.* **1996**, *35*, 6703.
[36] M. Filipic, P. Loper, B. Niesen, S. De Wolf, J. Krc, C. Ballif, M. Topic, *Opt. Express* **2015**, *23*, A263.
[37] H. Zhou, Q. Chen, G. Li, S. Luo, T.-B. Song, H.-S. Duan, Z. Hong, J. You, Y. Liu, Y. Yang, *Science* **2014**, *345*, 542.
[38] M. Saliba, T. Matsui, J. Y. Seo, K. Domanski, J. P. Correa-Baena, M. K. Nazeeruddin, S. M. Zakeeruddin, W. Tress, A. Abate, A. Hagfeldt, M. Gratzel, *Energy Environ. Sci.* **2016**, *9*, 1989.
[39] G. Kresse, J. Hafner, *Phys. Rev. B* **1993**, *47*, 558.
[40] G. Kresse, D. Joubert, *Phys. Rev. B* **1999**, *59*, 1758.
[41] J. P. Perdew, K. Burke, M. Ernzerhof, *Phys. Rev. Lett.* **1996**, *77*, 3865.
[42] J. Heyd, G. E. Scuseria, M. Ernzerhof, *J. Chem. Phys.* **2003**, *118*, 8207.
[43] A. V. Krukau, O. A. Vydrov, A. F. Izmaylov, G. E. Scuseria, *J. Chem. Phys.* **2006**, *125*, 224106.
[44] M. Gajdoš, K. Hummer, G. Kresse, J. Furthmüller, F. Bechstedt, *Phys. Rev. B* **2006**, *73*, 045112.